Targetome

ORIGINAL ARTICLE

Open Access

https://doi.org/10.48130/targetome-0026-0048

Targetome **2026**, 2(5): e048

Covalent targeting of IP receptor and PTEN mediates pyrrolizidine alkaloid-induced pulmonary hypertension

Caibin Zhang[#], Xiaokai Guo[#], Tianyang Huang[#], Yujian Fan and Yisheng He[*]

School of Medicine, The Chinese University of Hong Kong, Shenzhen, Guangdong 518172, China

[#] Authors contributed equally: Caibin Zhang, Xiaokai Guo, Tianyang Huang

[*] Correspondence: heyisheng@cuhk.edu.cn (He Y)

Abstract

Pulmonary arterial hypertension (PAH) is a progressive cardiopulmonary disorder characterized by obstructive pulmonary vascular remodeling and right ventricular dysfunction. Exposure to pyrrolizidine alkaloids (PAs), including monocrotaline (MCT), is a risk factor for PAH, yet the molecular targets of their reactive metabolite, dehydropyrrolizidine (DHP), remain incompletely defined. Using a rat model of MCT-induced PAH combined with untargeted proteomic profiling, covalent docking, targeted mass spectrometry, pharmacological intervention, and platelet-pulmonary arterial smooth muscle cell co-culture, we investigated DHP-mediated protein adduction in disease progression. Untargeted proteomic analysis identified multiple DHP-adducted proteins in platelets and lung tissues, with functional enrichment implicating platelet activation-related and proliferation-associated pathways. Targeted analyses demonstrated covalent modification of the platelet prostacyclin (IP) receptor at H237 in humans (H266 in rats), accompanied by reduced platelet cAMP levels and sustained platelet activation. In lung tissues, DHP covalently modified PTEN, including residue K125, consistent with disruption of its inhibitory control over PDGFR/PI3K signaling. *In vivo*, selexipag attenuated MCT-induced pulmonary vascular remodeling and reduced pulmonary PDGF-B accumulation and vascular cell proliferation. In parallel, dehydro-monocrotaline (the reactive form of MCT) stimulation of co-cultures containing platelets and rat pulmonary arterial smooth muscle cells (RPASMCs) increased P-selectin and PDGF levels, enhanced RPASMC proliferation, and activated PDGFR-β/PI3K/AKT signaling, whereas ACT-333679 attenuated these responses. Pharmacological upregulation of PTEN with rosiglitazone further suppressed PDGFR/PI3K signaling and pulmonary vascular remodeling. Collectively, these findings support a dual-target model in which DHP-mediated covalent modification of platelet IP receptor and pulmonary PTEN is associated with platelet dysregulation and proliferative vascular signaling in PA-induced PAH, and identify both pathways as potential therapeutic targets.

Keywords: Pulmonary arterial hypertension, Pyrrolizidine alkaloids, Monocrotaline, PTEN, IP receptor, Covalent modification, Covalent inhibitor

Citation: Zhang C, Guo X, Huang T, Fan Y, He Y. 2026. Covalent targeting of IP receptor and PTEN mediates pyrrolizidine alkaloid-induced pulmonary hypertension. *Targetome* 2(5): e048 https://doi.org/10.48130/targetome-0026-0048

Introduction

Pulmonary arterial hypertension (PAH) is a progressive and life-threatening cardiopulmonary disorder characterized by sustained elevation of pulmonary vascular resistance, ultimately leading to right ventricular failure[1]. Pathologically, PAH is characterized by obstructive remodeling of the precapillary pulmonary arteries, including intimal hyperplasia, medial hypertrophy, and, in advanced disease, plexiform lesions[2]. Historically, untreated PAH was associated with a poor prognosis, with a median survival of approximately 2.8 years[3]. Although contemporary therapeutic strategies have substantially improved long-term outcomes[4], PAH remains an incurable disease with considerable morbidity and mortality[5]. Most currently approved therapies primarily target pulmonary vasoconstriction and related symptoms but do not fully reverse the underlying vascular remodeling[6]. Therefore, identifying etiology-specific molecular drivers and therapeutically actionable pathways remains an important unmet need.

The etiology of PAH is heterogeneous, encompassing heritable, idiopathic, and associated forms, while exposure to certain drugs and toxins represents an increasingly recognized risk factor[7]. Among these environmental exposures, pyrrolizidine alkaloids (PAs) constitute a widespread class of naturally occurring phytotoxins found in approximately 6,000 plant species and have been implicated in the development of human PAH[8]. Human exposure occurs predominantly through contaminated foods and PA-containing herbal medicines, raising important concerns regarding their potential global health impact[8–10]. Recent ecological evidence further suggests that natural product exposures, including PA-containing herbal medicines and contaminated foods, may contribute to the regional and global burden of PAH, although these associations remain hypothesis-generating and require further validation[11].

Monocrotaline (MCT), a prototypical PA, is widely used to establish experimental PAH because of its reproducible pulmonary vascular toxicity[12,13]. MCT requires hepatic bioactivation to reactive dehydropyrrolizidine (DHP)-type metabolites, which contain electrophilic pyrrolic intermediates capable of forming covalent protein adducts[13]. Previous studies have primarily focused on DHP-induced pulmonary endothelial injury, inflammation, and subsequent vascular remodeling[8]. However, the protein targets covalently modified by DHP in the circulation and pulmonary vasculature remain incompletely defined. This knowledge gap limits our understanding of how systemic exposure to a single reactive metabolite can initiate and sustain the complex pathological processes underlying PA-induced PAH and hampers the identification of mechanism-based therapeutic targets.

Accumulating evidence indicates that platelet dysfunction contributes to PAH pathogenesis through enhanced platelet activation, thrombogenicity, and release of vasoactive and mitogenic mediators, including platelet-derived growth factor (PDGF), which can promote pulmonary vascular cell proliferation[8,14]. The prostacyclin (IP) receptor is a major inhibitory regulator of platelet activation and plays an essential role in maintaining platelet quiescence[15,16].

© The Author(s)

In parallel, phosphatase and tensin homolog (PTEN) is an important negative regulator of growth-promoting signaling, including the PDGFR/PI3K pathway, which is frequently dysregulated in pulmonary vascular remodeling[17,18]. These observations raise the possibility that covalent protein modification by DHP may simultaneously perturb platelet inhibitory signaling and pulmonary vascular proliferative control. We therefore hypothesized that the platelet IP receptor and pulmonary PTEN may represent functionally relevant covalent targets of DHP and that their coordinated disruption may contribute to a 'dual-hit' mechanism underlying PA-induced PAH.

In the present study, we combined a longitudinal rat model of MCT-induced PAH with untargeted proteomic profiling, covalent docking, targeted mass spectrometry, pharmacological intervention, and platelet-rat pulmonary arterial smooth muscle cell (RPASMC) co-culture to investigate the molecular consequences of DHP-mediated protein adduction. We first globally profiled DHP-adducted proteins in platelets and lung tissues without prior target-specific enrichment and then performed targeted validation of the IP receptor and PTEN as candidate covalent targets. We further examined whether modulation of IP receptor signaling with selexipag alters platelet-associated PDGF signaling and pulmonary vascular remodeling and used an *in vitro* platelet-RPASMC co-culture system to assess the relationship between dehydro-monocrotaline (DHMCT; the reactive form of MCT)-induced platelet activation, PDGF availability, and PDGFR/PI3K/AKT signaling. Finally, we evaluated whether pharmacological upregulation of PTEN with rosiglitazone could restore inhibitory control over proliferative signaling. Together, these approaches were designed to define how DHP-mediated covalent protein modification links systemic platelet dysfunction with pulmonary vascular proliferative signaling in PA-induced PAH.

Materials and methods

Animal model and treatment

Adult male Sprague–Dawley rats (6–8 weeks old, 180–200 g) were obtained from the Guangdong Provincial Animal Experiment Center. Animals were maintained in a climate-controlled facility under a 12-h light/dark cycle with *ad libitum* access to food and water. To establish the MCT-induced PAH model, MCT was initially dissolved in 1 mol·L^{-1} hydrochloric acid solution and subsequently neutralized to pH 7.0 using 1 mol·L^{-1} sodium hydroxide solution. The freshly prepared MCT solution was administered by intragastric gavage at a dose of 60 mg·kg^{-1} (Sigma-Aldrich, Cat# ST9H9BC12216, USA). MCT-exposed rats (n = 5 per time point for biochemical and molecular analyses) were euthanized at baseline and at 3, 9, 18, 30, and 48 h and 1, 2, 3, and 4 weeks after MCT administration. For immunohistochemical analyses and immunoblotting, three independent animals per group were used, and multiple sections or microscopic fields were quantified per animal. To evaluate the effects of selexipag on platelet-associated signaling and the development of MCT-induced PAH, an additional group of MCT-exposed rats (n = 5) received selexipag (NS-304; MedChemExpress, Cat# HY-14870, USA) once daily by oral gavage at a dose of 6 mg·kg^{-1}·day^{-1}. Selexipag treatment was initiated immediately after MCT administration and continued for 4 weeks. For the rosiglitazone treatment group (n = 5), rats received MCT (60 mg·kg^{-1}, gavage), followed immediately by daily intraperitoneal administration of rosiglitazone (10 mg·kg^{-1}; MedChemExpress, Cat# HY-17386, USA). Rosiglitazone treatment was initiated immediately after MCT administration and continued for 4 weeks. At the designated endpoints, blood, lung, and cardiac tissues were collected for subsequent analyses. Lung and cardiac tissues were fixed and paraffin-embedded for histopathological assessment, whereas anticoagulated whole blood was collected for platelet isolation and related analyses. All animal procedures were performed in accordance with protocols approved by the Animal Ethics Committee of The Chinese University of Hong Kong, Shenzhen (Approval No. CUHKSZ-AD-20230047; approved March 28, 2023).

Histopathological and immunohistochemical analysis

Lung and cardiac tissues were paraffin-embedded and sectioned at a thickness of 4 μm. Sections were subjected to hematoxylin and eosin (H&E) staining, and representative images were acquired using an inverted microscope (Nexcope NIB610-FL, China). Pulmonary artery wall thickness was determined according to the following equation:

$$Pulmonary\ artery\ wall\ thickness\ \% = \frac{Artery\ wall\ thickness \times 2}{Pulmonary\ artery\ diameter} \times 100\%$$

For pulmonary vascular remodeling analysis, pulmonary arteries were selected based on predefined morphological criteria. Only vessels with a clearly visible lumen and a near-circular cross-sectional profile were included to minimize measurement bias caused by oblique sectioning. Pulmonary arteries with an external diameter of approximately 20–100 μm were analyzed. For each animal, at least five pulmonary arteries were quantified. The analyses were not performed in a blinded manner.

Masson's trichrome staining was performed on cardiac sections using a Masson's Trichrome Kit (Servicebio, Cat# G1006, China) to assess collagen deposition. Briefly, sections were incubated with Masson A solution at 65 °C for 30 min, followed by sequential staining for nuclei (Masson B/C), cytoplasm (Masson D), and collagen (Masson F), with appropriate differentiation steps. The collagen-positive area, stained blue, was quantified using ImageJ software (v1.54g; National Institutes of Health, USA).

For immunohistochemical (IHC) staining, lung tissue sections were subjected to heat-induced antigen retrieval in citrate buffer (pH 6.0) and blocked with 10% goat serum for 1 h to minimize non-specific binding. Sections were subsequently incubated overnight at 4 °C with primary antibodies against von Willebrand factor (vWF; Abcam, Cat# ab287962, UK), α-smooth muscle actin (α-SMA; Servicebio, Cat# GB111364, China), PDGF-B (Servicebio, Cat# GB11261, China), phosphorylated PDGFR-β (p-PDGFR-β; Invitrogen, Cat# PA5-118659, USA), p-PI3K (Servicebio, Cat# GB150210, China), PTEN (Cell Signaling Technology, Cat# 9559S, USA), and Ki67 (Servicebio, Cat# GB121141, China). Following washing, sections were incubated with the appropriate peroxidase-conjugated secondary antibody (anti-rabbit IgG, Servicebio, Cat# G1302, China; or anti-mouse IgG, Servicebio, Cat# G1301, China) for 30 min at room temperature. Immunoreactivity was visualized using 3,3′-diaminobenzidine as the chromogenic substrate. The integrated optical density (IOD) of positively stained regions was quantified using ImageJ software (v1.54g; National Institutes of Health, USA).

Hemodynamic measurement and assessment of right ventricular hypertrophy

At 4 weeks after MCT administration, rats were anesthetized, and a Millar pressure catheter (Millar, USA) was introduced through the right jugular vein and advanced into the right ventricle. Right ventricular pressure signals were amplified using a Bridge Amp (FE221, ADInstruments, Australia) and recorded using an ADInstruments

data acquisition system. After stabilization of the pressure waveform, right ventricular systolic pressure (RVSP) was determined from the peak systolic pressure. Following hemodynamic measurements, the hearts were excised, and the right ventricular free wall (RV) was separated from the left ventricle plus interventricular septum (LV + S). The tissues were weighed separately, and right ventricular hypertrophy was assessed using the Fulton index, calculated as RV/(LV + S).

Quantification of pyrrole-protein adducts

Quantification of pyrrole-protein adducts was performed following previously established protocols[19,20]. In brief, proteins were isolated *via* acetone precipitation, after which the resulting pellet was subjected to incubation with 2% (w/v) acidic silver nitrate in ethanol for 30 min. Subsequently, the mixture underwent a derivatization reaction with 1% 4-(dimethylamino) benzaldehyde (in ethanol/perchloric acid) at 55 °C for 10 min. Following a 10-min centrifugation step at 15,000 × *g*, the clarified supernatant was harvested and subsequently examined using liquid chromatography-mass spectrometry (LC-MS).

Measurement of plasma free P-selectin

Platelet-poor plasma was prepared to minimize interference from residual platelets. Briefly, anticoagulated whole blood was centrifuged at 2,000 × *g* for 20 min at 4 °C immediately after collection. The resulting supernatant was then subjected to a second centrifugation at 10,000 × *g* for 10 min at 4 °C. P-selectin concentrations were quantified using a commercial ELISA kit (BYabscience, Cat# BY-ER330123, China) according to the manufacturer's instructions. Briefly, plasma samples were incubated in antibody-coated microplate wells at 37 °C for 60 min together with the horseradish peroxidase-conjugated detection antibody. Following washing, 3,3′-diaminobenzidine substrate was added, and the reaction was terminated using the supplied stop solution. Absorbance was measured at 450 nm using a microplate reader (FlexA-200, Allsheng, China).

Molecular docking

Covalent docking was performed using Maestro v12.8 (Schrödinger, Inc., New York, NY, USA). The carbonium-containing DHP molecule was prepared using LigPrep. Crystal structures of the IP receptor (PDB ID: 8X79) and PTEN (PDB ID: 7JUK) were obtained from the Protein Data Bank and processed using the Protein Preparation Wizard. Covalent docking was performed using the CovDock algorithm. Initial noncovalent binding poses were generated using Glide SP, followed by modeling of covalent bond formation. Positional restraints were applied to guide the electrophilic carbonium moiety of DHP toward candidate nucleophilic amino acid residues within the target protein, and covalent reactions were defined using a custom SMARTS pattern. The resulting docking poses were visualized using PyMOL (v1.6.0) and LigPlot+ (v2.2.8).

Platelet isolation

Platelets were isolated from whole blood using a Rat Peripheral Blood Platelet Isolation Kit (TBDscience, Cat# PLA2011RAT, China) according to the manufacturer's instructions. Briefly, 2 mL of whole blood was carefully layered onto 2 mL of separation medium in a sterile 5-mL glass tube and centrifuged at 275 × *g* for 15 min. The platelet-rich plasma layer was collected and, where applicable, diluted with an equal volume of sample diluent. The platelet suspension was subsequently centrifuged at 500 × *g* for 20 min to pellet the platelets. After removal of the supernatant, the isolated platelet pellet was processed for scanning electron microscopy or proteomic mass spectrometry analysis.

Scanning electron microscopy of platelets

Isolated platelets were fixed with an electron microscopy fixative (Servicebio, Cat# G1102, China) for 2 h and subsequently prepared for scanning electron microscopy (SEM) to assess platelet morphology and activation. SEM imaging was performed with technical assistance from Wuhan Servicebio Technology Co., Ltd.

Measurement of cAMP levels

Isolated platelets were subjected to ultrasonication, and the resulting lysates were used for cAMP quantification using a commercial ELISA kit (Elabscience, Cat# E-EL-0056, China) according to the manufacturer's instructions. Briefly, platelet lysates were added to microplate wells pre-coated with cAMP and incubated with a biotinylated anti-cAMP antibody for 45 min at 37 °C. After washing, TMB substrate solution was added, and the plates were incubated for 15 min at 37 °C in the dark. Absorbance was measured at 450 nm using a microplate reader (FlexA-200, Allsheng, China).

Platelet-RPASMC co-culture and assessment of platelet-mediated smooth muscle cell proliferation

Platelets were isolated from untreated Sprague–Dawley rats as described above and adjusted to a final concentration of 1×10^8 platelets/mL. Rat pulmonary arterial smooth muscle cells (RPASMCs; SNP-R043, Sunncell Biotechnology, Wuhan, China) were seeded into 96-well plates at a density of 1×10^4 cells/well and allowed to adhere before treatment. RPASMCs were subsequently co-cultured with freshly isolated platelets, and the co-cultures were assigned to three groups: control, DHMCT, and DHMCT + ACT-333679. The control group received vehicle alone, whereas the DHMCT group was treated with 100 μmol·L^{-1} DHMCT. For the DHMCT + ACT-333679 group, platelets were pretreated with 10 μmol·L^{-1} ACT-333679 (MedChemExpress, Cat# HY-79593, USA), the active metabolite of selexipag, for 30 min before exposure to 100 μmol·L^{-1} DHMCT. All co-cultures were incubated for 24 h at 37 °C in a humidified atmosphere containing 5% CO_2.

After 24 h of co-culture, culture supernatants were collected and centrifuged to remove residual cells and platelets. Plasma P-selectin concentrations were determined using a commercial ELISA kit (BYabscience, Cat# BY-ER330123, China), and PDGF concentrations were measured using a commercial rat PDGF ELISA kit (mlbio, Cat# ml106793, China), according to the manufacturers' instructions. RPASMC proliferation was assessed using a Cell Counting Kit-8 (CCK-8; Solarbio, Cat# CA1210, China). Following the 24-h co-culture period, CCK-8 reagent was added according to the manufacturer's instructions, and cell proliferation was expressed relative to the control group.

For analysis of proliferative signaling, parallel RPASMC cultures were established under the same treatment conditions. After 24 h, the culture medium and platelets were removed, and RPASMCs were washed with phosphate-buffered saline and lysed in RIPA buffer supplemented with protease and phosphatase inhibitors. The resulting protein samples were subjected to western blot analysis. Membranes were incubated overnight at 4 °C with primary antibodies against phosphorylated PDGFR-β (p-PDGFR-β; Thermo Fisher

Scientific, Cat# PA5-118659, USA), phosphorylated PI3K (p-PI3K; Servicebio, Cat# GB150210, China), phosphorylated AKT (p-AKT; Cell Signaling Technology, Cat# 4060T, USA), and GAPDH (Servicebio, Cat# GB15004, China). Following washing, membranes were incubated with appropriate horseradish peroxidase-conjugated secondary antibodies. Protein bands were visualized using an enhanced chemiluminescence detection system, with GAPDH used as the loading control.

Global proteomic profiling of DHP-adducted proteins and functional enrichment analysis

To globally profile potential protein targets of reactive MCT metabolites without prior target selection, platelets and lung tissues collected from MCT-exposed rats were subjected directly to untargeted proteomic analysis without immunoprecipitation or other target-specific enrichment. Platelet pellets and homogenized lung tissues were lysed, and total proteins were extracted and quantified. Equal amounts of protein from each sample were digested with sequencing-grade trypsin for 15 h at 37 °C. The resulting peptides were analyzed by liquid chromatography-tandem mass spectrometry (LC-MS/MS) using an Orbitrap Exploris 480 mass spectrometer (Thermo Fisher Scientific, USA).

Raw LC-MS/MS data were processed using Proteome Discoverer software (v2.4; Thermo Fisher Scientific, USA) and searched against the *Rattus norvegicus* proteome database. To identify proteins covalently modified by reactive MCT metabolites, a pyrrole moiety adduct corresponding to a mass shift of +135.0684 Da was included as a variable modification during database searching. Proteins containing at least one peptide carrying the +135.0684 Da modification were considered candidate DHP-adducted proteins. In contrast to the subsequent targeted co-immunoprecipitation-mass spectrometry analysis of the IP receptor and PTEN, this global analysis was performed directly on total platelet and lung proteins without enrichment for any predefined protein target.

DHP-adducted proteins identified in platelets and lung tissues were analyzed separately using the Metascape platform. Gene identifiers corresponding to the identified proteins were submitted for pathway, biological process, and disease-associated enrichment analyses using annotation resources including Gene Ontology (GO), Reactome, and DisGeNET, as appropriate. Enriched terms were ranked according to statistical significance and visualized based on $-\log_{10}(p)$ values.

Targeted proteomic mass spectrometry and site-specific mapping of DHP adducts

To validate candidate covalent targets and characterize DHP-modified amino acid residues, the IP receptor and PTEN were separately enriched by co-immunoprecipitation from platelet lysates and homogenized lung tissue lysates, respectively. Briefly, lysates were incubated with magnetic beads (Sigma-Aldrich, Cat# LSKMAGA10, USA) pre-coated with anti-IP receptor antibody (Santa Cruz Biotechnology, Cat# sc-365268, USA) or anti-PTEN antibody (Cell Signaling Technology, Cat# 9559S, USA), according to the manufacturer's co-immunoprecipitation protocol. Following immunoprecipitation and protein enrichment, samples were subjected to proteomic sample preparation prior to LC-MS/MS analysis. The enriched proteins were diluted with 50 mmol·L^{-1} ammonium bicarbonate buffer and reduced by incubation with 10 mmol·L^{-1} tris(2-carboxyethyl)phosphine (TCEP) at 55 °C for 1 h. After cooling to room temperature, samples were alkylated with 20 mmol·L^{-1} iodoacetamide (IAA) in the dark for 30 min. The resulting proteins were digested with trypsin at an enzyme-to-substrate ratio of 1 : 50 (w/w) at 37 °C overnight (~15 h). The generated peptides were subsequently subjected to LC-MS/MS analysis.

Raw MS data were analyzed using Proteome Discoverer 2.4 (Thermo Fisher Scientific). Database searches were performed against the UniProt protein database with dynamic modifications including oxidation (M), acetylation (N-terminal), methionine loss (M), carbamidomethylation (C), and DHP adduct modification (C, H, K, R, D, and E). Peptide-spectrum matches (PSMs) were filtered according to predefined confidence criteria, and only high-confidence PSMs with confident site localization were included for subsequent analysis.

The frequency of DHP-adducted residues was calculated based on the relative occurrence of confidently identified DHP-modified residues among all qualified DHP-adduct identifications. Only high-confidence PSMs with confident site localization were included, and only amino acid residues identified as DHP adducts in more than one independent identification event were considered for frequency calculation. These values were interpreted as relative modification frequencies and were used to compare the distribution patterns of DHP adduction rather than to represent absolute site-specific chemical reactivity.

Statistical analysis

Statistical analyses were performed using GraphPad Prism software (v9.0.0; GraphPad Software, USA). Data are presented as mean ± SD. For experiments involving comparisons between a single MCT-treated time point and the corresponding control group, differences between two independent groups were evaluated using an unpaired two-tailed Student's *t*-test. A two-sided P-value < 0.05 was considered statistically significant.

Results

MCT exposure induces pulmonary vascular remodeling and right ventricular hypertrophy

To evaluate the structural changes in pulmonary vasculature following MCT administration, we performed a longitudinal histological assessment of lung tissues over a 4-week period. H&E staining of lung sections revealed prominent thickening of the pulmonary arterial wall (Fig. 1a). IHC staining further demonstrated marked changes in both the endothelial layer, as indicated by increased von Willebrand factor (vWF) expression (Fig. 1b), and the medial smooth muscle layer, highlighted by enhanced α-smooth muscle actin (α-SMA) staining (Fig. 1c). Quantitative analyses confirmed significant increases in total arterial wall thickness, endothelial layer thickness, and medial smooth muscle layer thickness compared with controls (Fig. 1d–f). Together, these results demonstrate that MCT exposure induces robust and progressive pulmonary vascular remodeling, characterized by concurrent endothelial hyperplasia and medial smooth muscle hypertrophy.

Consistent with the development of PAH, MCT administration led to progressive structural remodeling of the right ventricle. Representative whole-heart sections stained with H&E demonstrated noticeable right ventricular hypertrophy and thickening of the right ventricular wall over time, evident from 1 to 4 weeks after MCT treatment compared with the control group (Supplementary Fig. S1a and S1b). Masson's trichrome staining revealed a

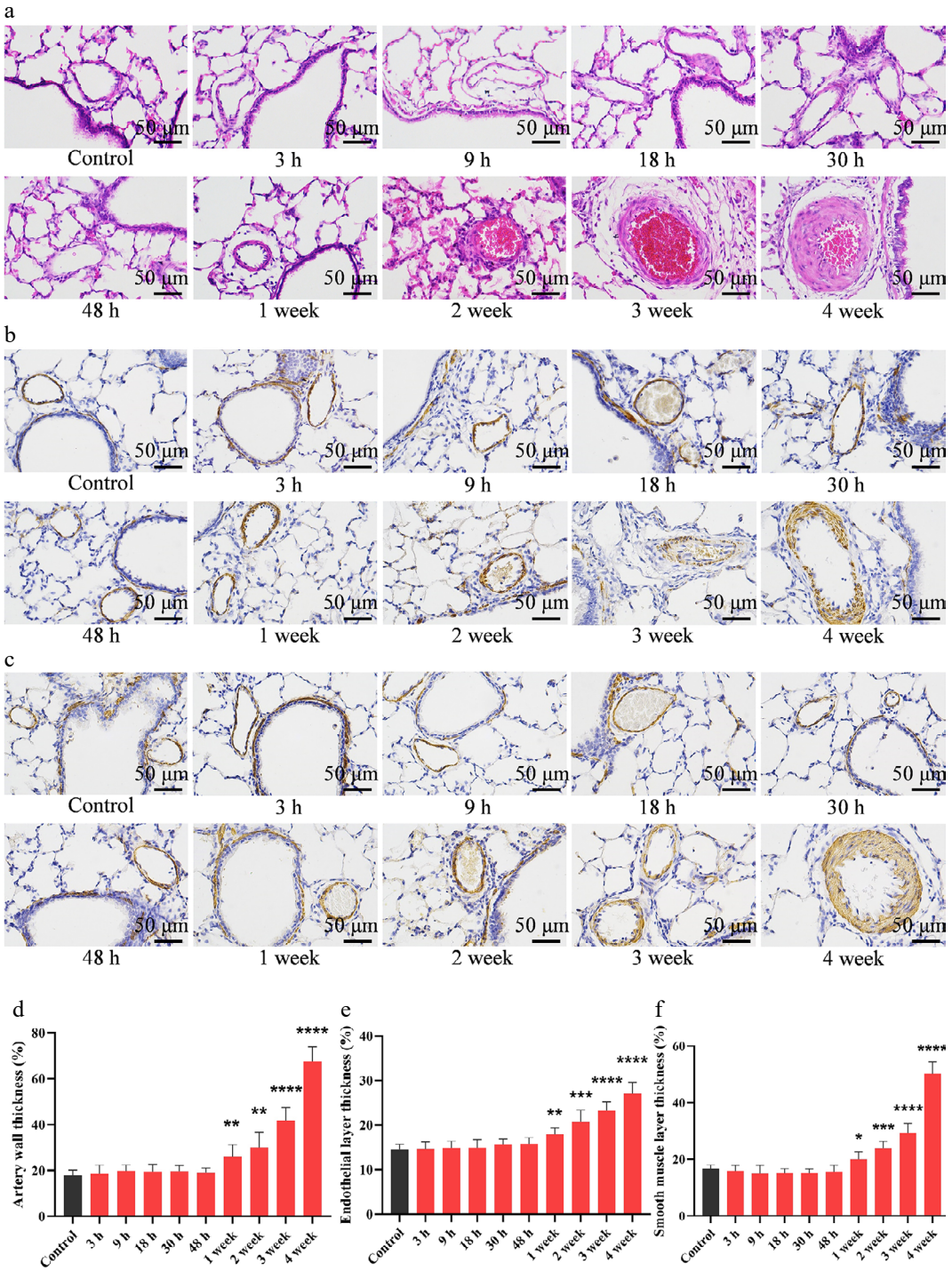


Fig. 1 MCT exposure triggers pulmonary vascular remodeling. (a) Representative images of H&E-stained lung sections from MCT-treated rats, showing prominent thickening of the pulmonary arterial wall. Representative immunohistochemical staining for (b) vWF and (c) α-SMA in lung tissues, highlighting changes in the endothelial and medial smooth muscle layers, respectively. Quantitative analysis of (d) total pulmonary arterial wall thickness, (e) vWF-positive endothelial layer thickness, and (f) α-SMA-positive medial smooth muscle layer thickness. Data are presented as mean ± SD (n = 3). * P < 0.05, ** P < 0.01, *** P < 0.001, **** P < 0.0001 compared with the control group (unpaired Student's t-test). Scale bar = 50 μm.

marked increase in collagen deposition (stained blue) within the right ventricular myocardium, indicating the development of interstitial fibrosis following MCT exposure (Supplementary Fig. S1c). These morphological changes were corroborated by quantitative measurements showing significant increases in right ventricular wall thickness and collagen-positive area (Supplementary Fig. S1d and S1e). Consistent with the histological evidence of right ventricular hypertrophy, the Fulton index was significantly increased in MCT-exposed rats at week 4 compared with controls (Supplementary Fig. S1f). Hemodynamic assessment further revealed a marked elevation in RVSP in MCT-exposed rats, as demonstrated by representative pressure tracings and quantitative analysis (Supplementary Fig. S1g and S1h). Together, these findings demonstrate that MCT induces significant pulmonary hypertension accompanied by right ventricular hypertrophy and fibrosis, key pathological features of PAH.

Reactive MCT metabolites covalently modify circulating proteins and trigger platelet activation

To investigate the systemic hematological effects of MCT exposure, we first measured the formation of pyrrole-protein adducts in whole blood, which reflect the covalent binding of reactive MCT metabolites to circulating proteins. Following MCT administration, these adducts were rapidly detected within 3 h and exhibited a progressive increase, reaching a peak at 48 h post-exposure. Although the concentrations gradually declined thereafter, the adducts persisted at high levels throughout the 4-week study period (Fig. 2a). Collectively, these data suggest systemic exposure to the reactive metabolite dehydropyrrolizidine (DHP) and its interaction with the hematologic compartment. We next assessed whether this systemic exposure was associated with hematologic dysfunction by monitoring plasma P-selectin, a sensitive marker of platelet activation. Consistent with the temporal profile of pyrrole-protein adduct formation, plasma P-selectin levels showed a significant rise starting at 9 h ($P < 0.05$) and peaked at 48 h post-MCT exposure ($P < 0.01$). Notably, this activated platelet state persisted into the later stages of the experiment, with significantly elevated P-selectin levels maintained through week 4 ($P < 0.05$) (Fig. 2b). Consistent with these biochemical findings, scanning electron microscopy revealed time-dependent morphological changes characteristic of platelet activation following MCT exposure (Fig. 2c). Compared with the smooth, discoid morphology of control platelets, MCT-exposed platelets exhibited progressive shape irregularity and the formation of increasingly prominent pseudopodia over time.

To further characterize the protein targets of reactive MCT metabolites in platelets at a broader proteome-wide level, total platelet proteins from MCT-exposed rats were subjected directly to untargeted proteomic mass spectrometry without prior immunoprecipitation or target-specific enrichment. This analysis identified a broad spectrum of DHP-adducted platelet proteins, which are summarized in Supplementary Table S1. Functional enrichment analysis of these identified proteins using Metascape revealed significant enrichment of multiple biological pathways, including the Reactome pathway 'Platelet activation, signaling and aggregation' (Fig. 2d). These proteomic findings further support a close association between covalent modification of platelet proteins by reactive MCT metabolites and platelet activation. Collectively, these biochemical, morphological, and proteomic findings indicate that circulating MCT metabolites covalently modify platelet proteins and trigger early and sustained platelet activation, establishing a critical systemic link that may contribute to subsequent pulmonary vascular damage and remodeling.

MCT metabolites directly bind and covalently modify the platelet IP receptor to trigger activation

To investigate the mechanistic link between systemic MCT metabolites and platelet dysfunction, we examined the interaction between DHP and the IP receptor, a G-protein-coupled receptor known to inhibit platelet aggregation[21]. Given its essential role in maintaining platelet quiescence, the IP receptor was considered a primary candidate for DHP-mediated interference. Our molecular docking studies revealed histidine residue 237 of the human IP receptor (corresponding to H266 in rats) as a candidate DHP-interacting residue (Fig. 3a). To experimentally validate the direct interaction between DHP and the IP receptor, we performed mass spectrometry-based proteomic analysis of the IP receptor purified from platelets of MCT-exposed rats. The analysis revealed direct covalent modification of specific amino acid residues by DHP. A representative MS/MS spectrum confirmed DHP adduction at residue H266 of the IP receptor (Fig. 3b). Broader proteomic mapping further identified multiple DHP-modified residues throughout the receptor sequence, including R204, R248, H249, R258, R260, E261, E263, H266, and R287 (Fig. 3c). Detailed PSM information supporting these identified DHP modification sites is provided in Supplementary Table S2. Sequence alignment analysis using UniProt demonstrated high conservation between human and rat IP receptors, with the DHP-modified residue identified in the rat IP receptor (H266) corresponding to human H237 used for structural modeling (Fig. 3d and Supplementary Fig. S2). Functionally, platelets from MCT-exposed rats exhibited significantly decreased cAMP levels, supporting the possibility that DHP modification may impair IP receptor signaling (Fig. 3e).

Together, these computational and experimental results suggest that DHP does not merely occupy the receptor but forms a covalent modification that may contribute to sustained attenuation of IP receptor signaling. Given that the IP receptor normally maintains platelets in a quiescent state[22], its covalent modification by DHP may impair IP receptor signaling and is consistent with the sustained platelet activation observed in our model.

MCT exposure is associated with pulmonary PDGF-B accumulation and activation of the PDGFR/PI3K proliferative pathway

To investigate whether platelet activation is associated with changes in pulmonary PDGF-B signaling and vascular remodeling, we first examined the expression and localization of Platelet-Derived Growth Factor-B (PDGF-B) in lung tissues. Immunohistochemical staining revealed a time-dependent increase in PDGF-B expression within the walls of pulmonary arteries, beginning at 18 h and becoming pronounced at 1–4 weeks post-MCT administration (Fig. 4a). This accumulation of PDGF-B was accompanied by the activation of its cognate receptor, as evidenced by elevated levels of phosphorylated PDGFR in lung tissues over the same time course (Fig. 4b). Concurrently, expression of the downstream signaling molecule PI3K was also progressively upregulated in a progressive manner (Fig. 4c). The functional outcome of this sustained PDGFR/PI3K pathway activation was a significant increase in cellular proliferation within the pulmonary vasculature. Ki67 staining demonstrated a time-dependent rise in the number of proliferating cells in the lung sections of MCT-treated rats, peaking at the later stages of exposure (Fig. 4d). Collectively, these temporal changes demonstrate a close association between MCT exposure, pulmonary PDGF-B accumulation, PDGFR/PI3K activation, and vascular cell proliferation, prompting us to further investigate the functional contribution of platelet activation using pharmacological intervention and an *in vitro* co-culture system.

Selexipag attenuates MCT-induced pulmonary vascular remodeling and suppresses platelet activation-associated PDGF/PDGFR/PI3K/AKT signaling

To further evaluate whether pharmacological modulation of the platelet-associated IP receptor pathway affects the downstream pulmonary vascular phenotype, MCT-exposed rats were treated with selexipag. Histopathological examination showed that MCT exposure induced marked pulmonary arterial wall thickening, whereas selexipag treatment substantially attenuated this structural

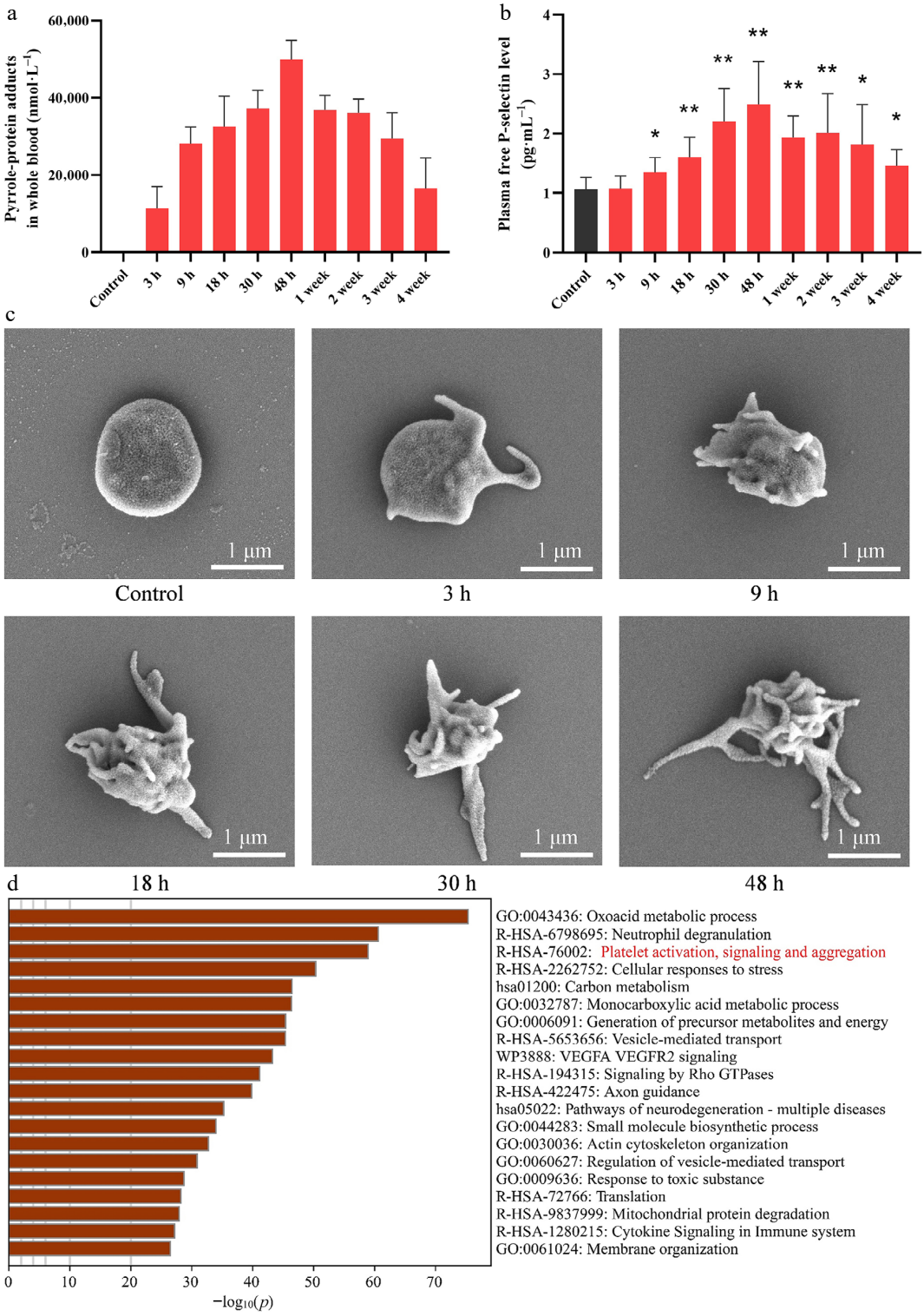


Fig. 2 MCT metabolites form covalent adducts with blood proteins and trigger platelet activation. (a) Levels of pyrrole-protein adducts in whole blood following MCT exposure. (b) Plasma free P-selectin concentrations following MCT exposure, reflecting time-dependent platelet activation. (c) Representative scanning electron microscopy images of platelets isolated from control and MCT-exposed rats at different time points. Compared with the smooth, discoid morphology of control platelets, platelets from MCT-exposed rats progressively exhibited morphological features of activation, including shape irregularity and the formation of increasingly prominent pseudopodia. Scale bar = 1 μm. (d) Metascape pathway enrichment analysis of DHP-adducted proteins identified by untargeted proteomic mass spectrometry in platelets from MCT-exposed rats, revealing significant enrichment of pathways associated with platelet activation, signaling, and aggregation. For (a) and (b), data are presented as mean ± SD (n = 5). * P < 0.05, ** P < 0.01 vs. the control group (unpaired Student's t-test).

remodeling (Fig. 5a). Consistently, immunohistochemical staining for vWF and α-SMA demonstrated pronounced endothelial hyperplasia and medial smooth muscle hypertrophy in MCT-exposed rats, both of which were significantly reduced following selexipag treatment. Quantitative analyses confirmed decreases in total pulmonary arterial wall thickness, endothelial layer thickness, and smooth

https://doi.org/10.48130/targetome-0026-0048

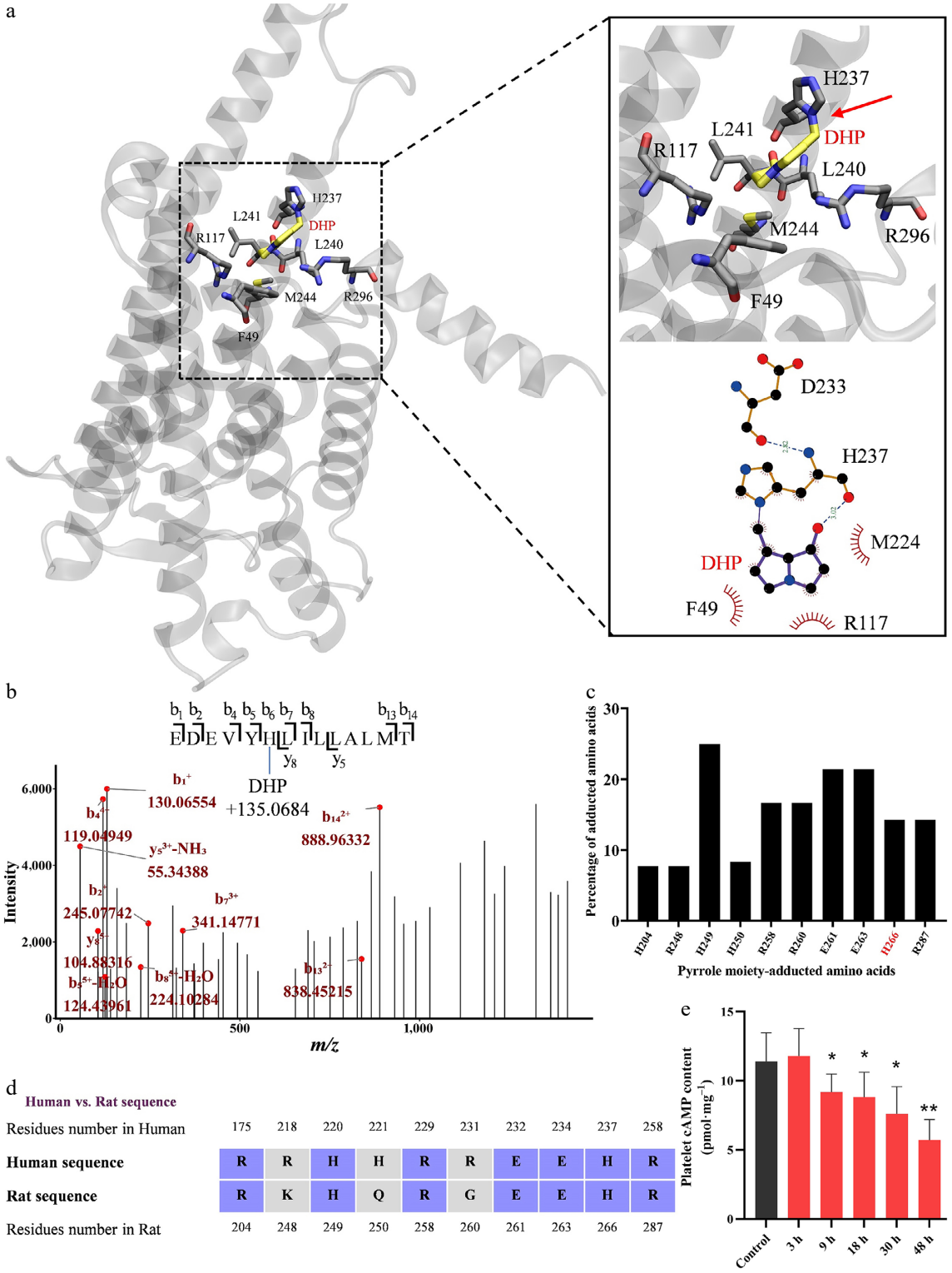


Fig. 3 The active MCT metabolite dehydropyrrolizidine (DHP) directly binds to the IP receptor, as demonstrated by molecular docking and proteomic analysis. (a) Molecular docking suggests a stable interaction between DHP and residue H237 of the human IP receptor (corresponding to H266 in rats). (b) Proteomic mass spectrometry analysis of the IP receptor purified from platelets of MCT-exposed rats identifies covalent modification of specific amino acid residues by DHP. A representative mass spectrum confirms DHP adduction to residue H266 (b_6), corresponding to human H237. (c) Summary of DHP-modified residues identified across the IP receptor protein. (d) Sequence alignment of rat and human IP receptors showing that the DHP-modified residue H266 in rats is conserved in humans. (e) Decreased cAMP levels in platelets from MCT-exposed rats further support DHP-mediated inhibition of the IP receptor. Data are presented as mean ± SD ($n = 5$). * $P < 0.05$, ** $P < 0.01$ vs. the control group (unpaired Student's t-test).

muscle layer thickness in the selexipag-treated group compared with the MCT-exposed group (Fig. 5a). Importantly, MCT exposure was accompanied by a marked increase in PDGF-B accumulation within the pulmonary vascular wall, whereas selexipag treatment significantly reduced pulmonary vascular PDGF-B expression (Fig. 5b). In parallel, the increased number of Ki67-positive cells observed in

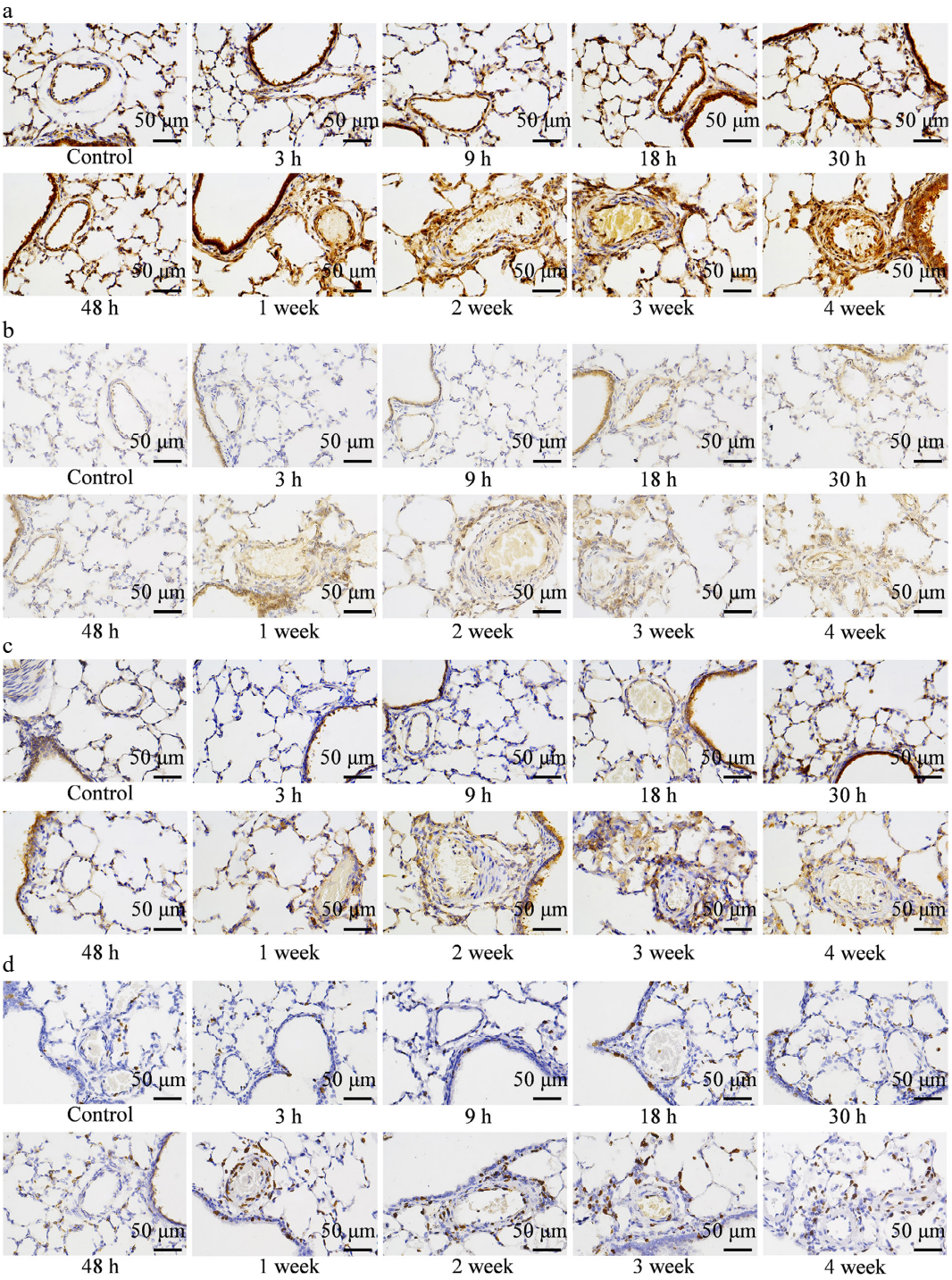


Fig. 4 MCT-induced platelet activation promotes PDGF-B accumulation and activates the PDGFR/PI3K signaling pathway in lung tissues. (a) Representative images of IHC staining for PDGF-B, showing increased PDGF-B expression in pulmonary arteries of MCT-exposed rats. Representative images of (b) p-PDGFR and (c) p-PI3K expression in lung tissues, indicating activation of the PDGFR/PI3K cascade. (d) Ki67 staining in lung sections, demonstrating enhanced cellular proliferation in response to PDGFR/PI3K pathway upregulation. Scale bar = 50 μm.

MCT-exposed pulmonary vessels was markedly decreased after selexipag treatment, indicating attenuation of abnormal vascular cell proliferation (Fig. 5b). Collectively, these intervention data show that selexipag ameliorates MCT-induced pulmonary vascular remodeling and is associated with reduced PDGF-B accumulation and vascular cell proliferation, supporting the involvement of the platelet/IP receptor-PDGF axis in the development of MCT-induced PAH.

To further determine whether activated platelets directly contribute to pulmonary arterial smooth muscle cell proliferation, we established an *in vitro* co-culture system using platelets isolated from untreated rats and RPASMCs. Exposure to DHMCT markedly increased P-selectin levels in the culture supernatant, indicating enhanced platelet activation, and was accompanied by a significant increase in supernatant PDGF concentrations (Supplementary Fig. S3a and S3b). Consistent with these changes, DHMCT treatment

https://doi.org/10.48130/targetome-0026-0048

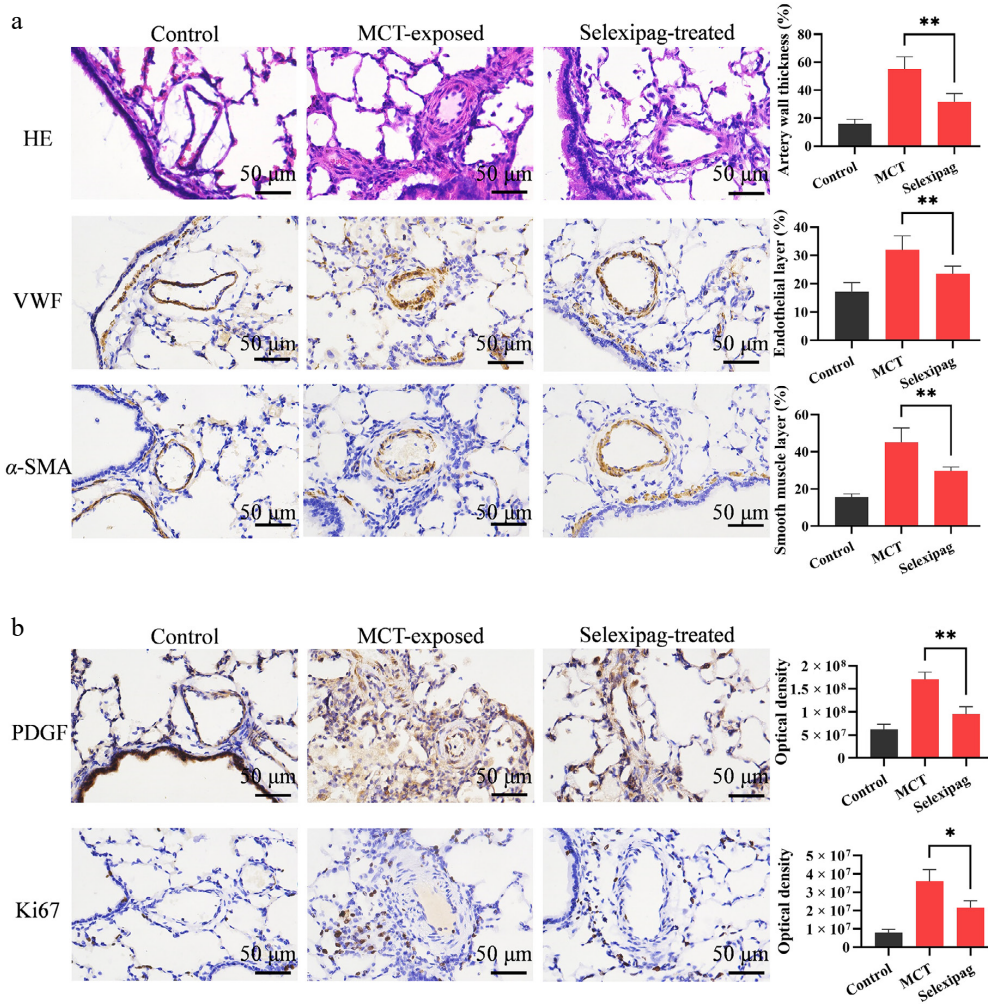


Fig. 5 Selexipag attenuates MCT-induced pulmonary vascular remodeling and reduces pulmonary PDGF-B accumulation and vascular cell proliferation. (a) Representative H&E staining and immunohistochemical staining for vWF and α-SMA in lung tissues from control, MCT-exposed, and selexipag-treated rats. MCT exposure induced marked pulmonary arterial wall thickening, endothelial hyperplasia, and medial smooth muscle hypertrophy, whereas selexipag treatment attenuated these pathological changes. Quantitative analyses of pulmonary arterial wall thickness, endothelial layer thickness, and smooth muscle layer thickness are shown on the right. (b) Representative immunohistochemical staining and quantitative analyses of PDGF-B and Ki67 in pulmonary arteries. MCT exposure markedly increased pulmonary vascular PDGF-B accumulation and the number of proliferating Ki67-positive cells, whereas selexipag treatment significantly reduced PDGF-B expression and vascular cell proliferation. Data are presented as mean ± SD (n = 3). * P < 0.05, ** P < 0.01 vs. the MCT-exposed group (unpaired Student's t-test). Scale bar = 50 μm.

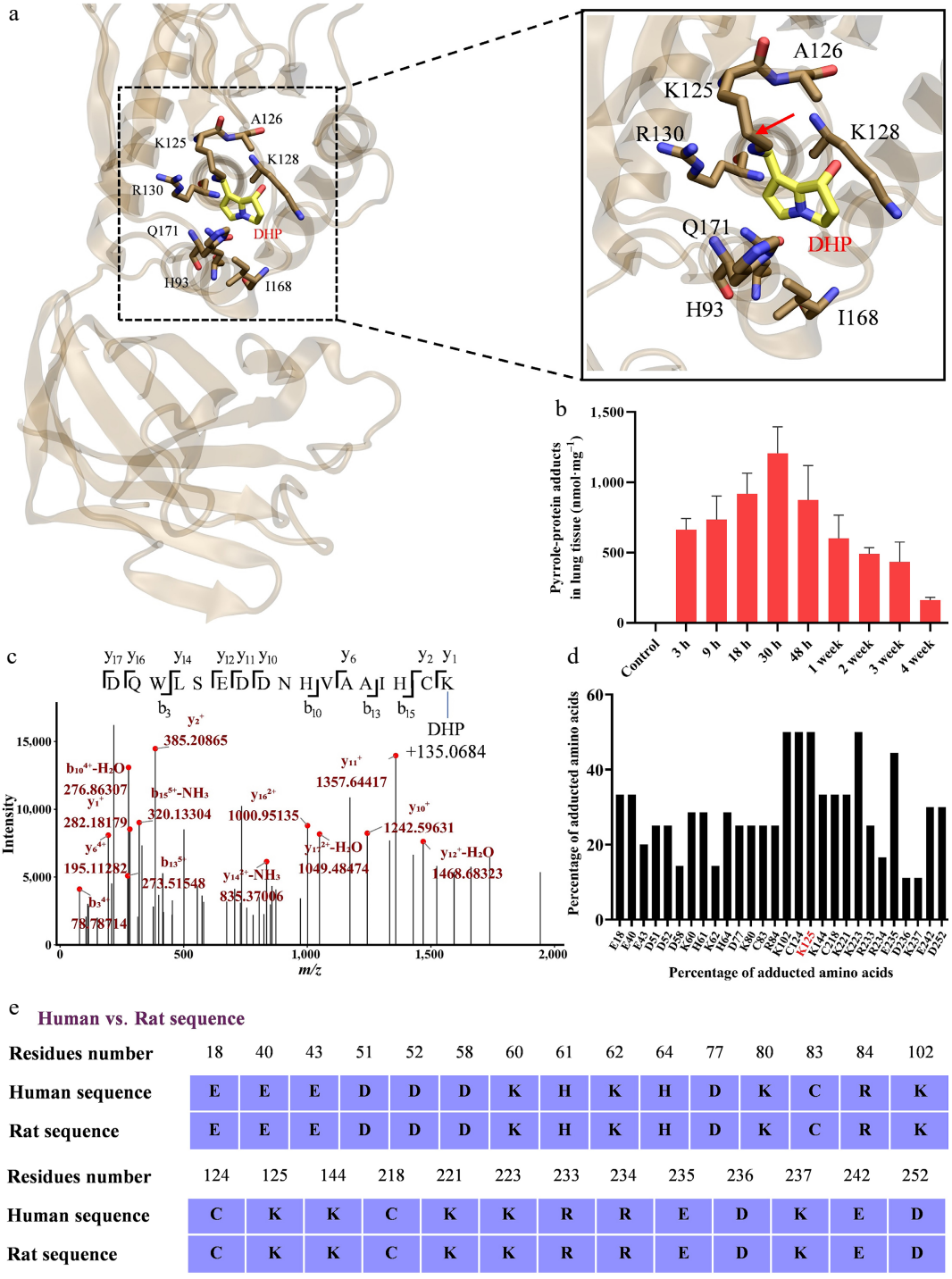
significantly enhanced RPASMC proliferation, as assessed by the CCK-8 assay (Supplementary Fig. S3c). At the signaling level, western blot analysis showed that DHMCT treatment increased the phosphorylation of PDGFR-β, PI3K, and AKT in RPASMCs, indicating activation of the PDGFR/PI3K/AKT proliferative signaling cascade (Supplementary Fig. S3d). Importantly, pretreatment with ACT-333679, the active metabolite of selexipag, attenuated DHMCT-induced increases in P-selectin and PDGF levels, reduced RPASMC proliferation, and suppressed phosphorylation of PDGFR-β, PI3K, and AKT. These *in vitro* findings provide mechanistic support for a functional link between DHMCT-induced platelet activation, increased PDGF availability, activation of PDGFR/PI3K/AKT signaling in RPASMCs, and enhanced smooth muscle cell proliferation.

PTEN is identified as a direct target of MCT adduction in the lung, leading to its functional impairment

To broadly characterize the pulmonary protein targets of reactive MCT metabolites without prior target selection, total proteins extracted from lung tissues of MCT-exposed rats were subjected directly to untargeted proteomic mass spectrometry without prior co-immunoprecipitation or target-specific enrichment. This analysis identified a broad spectrum of DHP-adducted proteins in lung tissues, which are summarized in Supplementary Table S3. Metascape-based DisGeNET enrichment analysis of these proteins revealed significant associations with multiple disease-related terms, including several cancer-related categories, such as anaplastic carcinoma, carcinomatosis, and undifferentiated carcinoma (Supplementary Fig. S4). This enrichment pattern prompted us to focus on DHP-adducted proteins with established roles in the regulation of abnormal cellular growth and proliferation. Notably, PTEN, a key negative regulator of proliferative signaling, was identified among the DHP-adducted proteins in lung tissues.

Given that PTEN negatively regulates the PDGFR/PI3K signaling axis[23,24], which was markedly activated following MCT exposure, we hypothesized that covalent modification of PTEN by DHP might contribute to the dysregulation of this proliferative pathway. To investigate this possibility, we first performed molecular docking to

assess the potential interaction between DHP and PTEN. The analysis revealed a representative binding mode in which DHP fits into the active pocket of PTEN and forms a covalent bond with residue K125 (Fig. 6a). To determine whether such interactions occur in a biological context, we next examined the formation of pyrrole-protein adducts in lung tissues from MCT-exposed rats. A marked accumulation of these adducts was observed, indicating substantial DHP-protein binding *in vivo* (Fig. 6b). To further validate PTEN as a direct covalent target, PTEN was purified from lung tissues of MCT-exposed rats and subjected to targeted proteomic mass spectrometry. This analysis confirmed DHP modification of PTEN at K125 (Fig. 6c). Peptide mapping further revealed multiple DHP-adducted residues, with K125 emerging as a prominent modification site (Fig. 6d). Detailed PSM information supporting the identified PTEN



Residues number	18	40	43	51	52	58	60	61	62	64	77	80	83	84	102
Human sequence	E	E	E	D	D	D	K	H	K	H	D	K	C	R	K
Rat sequence	E	E	E	D	D	D	K	H	K	H	D	K	C	R	K

Residues number	124	125	144	218	221	223	233	234	235	236	237	242	252
Human sequence	C	K	K	C	K	K	R	R	E	D	K	E	D
Rat sequence	C	K	K	C	K	K	R	R	E	D	K	E	D

Fig. 6 Molecular docking and proteomic analysis identify PTEN as a direct target of DHP. (a) Covalent docking model illustrating covalent bond formation between DHP and the K125 residue of PTEN. (b) Concentration of pyrrole-protein adducts in rat lung tissues following MCT exposure, demonstrating the protein-binding capacity of DHP *in vivo*. (c) Representative MS/MS spectrum of PTEN purified from MCT-exposed rat lung tissue, confirming the covalent modification of K125 by DHP. (d) Summary of DHP-modified residues identified by proteomic analysis within the PTEN protein sequence. (e) Sequence alignment of rat and human PTEN shows that all DHP-modified amino acid residues are conserved between the two species.

DHP modification sites is provided in Supplementary Table S4. Notably, clinical variants involving nearly all of these identified DHP-adducted residues are classified as pathogenic in the UniProt database[25,26]. This correlation suggests that these structurally relevant residues may contribute to DHP-mediated perturbation of PTEN function. In addition, sequence alignment demonstrated that all DHP-modified residues are conserved between rat and human PTEN (Fig. 6e). Together, these results demonstrate that DHP directly targets and covalently modifies PTEN at the K125 residue, providing a molecular mechanism underlying the loss of PTEN-mediated suppression of the PDGFR/PI3K proliferative axis in MCT-induced PAH.

Rosiglitazone treatment is associated with increased PTEN expression and attenuation of PDGFR/PI3K signaling during MCT-induced pulmonary vascular remodeling

To evaluate whether pharmacological modulation associated with increased PTEN expression affects the PDGFR/PI3K signaling axis, we treated MCT-exposed rats with rosiglitazone (ROSI), a PPARγ agonist previously reported to regulate PTEN expression[27]. Histopathological and IHC analyses revealed that ROSI treatment significantly attenuated the pulmonary vascular remodeling triggered by MCT. Compared with the MCT-exposed group, H&E staining showed a marked reduction in pulmonary arterial wall thickness in ROSI-treated rats. Consistent with this structural improvement, immunohistochemistry for vWF and α-SMA demonstrated that ROSI alleviated both the endothelial hyperplasia and the medial smooth muscle hypertrophy characteristic of MCT exposure (Fig. 7a).

Mechanistically, ROSI treatment was associated with increased PTEN expression in lung tissues and reduced activation of the PDGFR/PI3K signaling axis compared with MCT exposure (Fig. 7b, top panel). This restoration of PTEN was associated with a significant downregulation of the previously activated PDGFR/PI3K signaling axis. Quantitative analysis confirmed that levels of phosphorylated PDGFR (p-PDGFR) and PI3K were substantially reduced in the ROSI-treated group compared with the MCT group (Fig. 7b, middle panels). Consequently, this inhibition of the proliferative signaling cascade led to a marked decrease in vascular cell proliferation, as evidenced by a significant reduction in Ki67-positive cells within the pulmonary vasculature of ROSI-treated animals (Fig. 7b, bottom panel). Collectively, these findings indicate that rosiglitazone treatment is associated with increased PTEN expression, reduced PDGFR/PI3K signaling activation, and attenuation of vascular cell proliferation.

Discussion

Pulmonary arterial hypertension induced by pyrrolizidine alkaloids such as MCT provides a well-established model for investigating toxin-associated pulmonary vascular remodeling. Although hepatic bioactivation of MCT to the reactive metabolite DHP is known to be required for toxicity, the molecular targets through which DHP perturbs systemic and pulmonary vascular homeostasis remain incompletely understood. In this study, we identified two functionally relevant classes of DHP targets: the platelet IP receptor and the pulmonary PTEN pathway. Previous studies of MCT-induced PAH have extensively characterized downstream pathological processes, including endothelial injury, inflammatory responses, platelet activation, PDGF signaling, and dysregulation of vascular proliferative pathways. However, the molecular events that initiate these downstream alterations following exposure to reactive MCT metabolites remain incompletely understood. In the present study, we identified site-specific covalent modification of the platelet IP receptor and pulmonary PTEN by the reactive metabolite DHP as a previously unrecognized molecular mechanism linking environmental toxicant exposure to pulmonary vascular remodeling. Rather than simply demonstrating the involvement of established PAH-associated pathways, our study reveals that DHP may act as a molecular initiator by directly modifying key regulatory proteins, thereby triggering persistent platelet activation and disrupting PTEN-mediated inhibition of proliferative signaling. These findings provide a mechanistic framework in which reactive metabolite-induced covalent protein modification serves as an upstream event driving MCT-induced PAH pathogenesis.

Traditionally, the pulmonary toxicity of MCT has been attributed predominantly to hepatic bioactivation followed by pulmonary endothelial injury and inflammation[8]. Our findings extend this model by demonstrating a substantial systemic hematological component. Pyrrole-protein adducts were detected rapidly after MCT exposure and persisted for several weeks, accompanied by sustained elevation of soluble P-selectin and progressive morphological changes characteristic of platelet activation. Direct untargeted proteomic analysis of total platelet proteins further identified a broad spectrum of candidate DHP-adducted proteins, with functional enrichment including the Reactome pathway 'Platelet activation, signaling, and aggregation'. These findings are consistent with previous reports showing pulmonary platelet sequestration[28], increased fibrinogen-binding platelets[29], enhanced platelet–neutrophil interactions[29], increased platelet-activating factor[30], and increased platelet surface CD62P[31] in MCT-induced PAH (Supplementary Table S5). Together, these observations support sustained platelet dysregulation as an important systemic component of MCT-induced pulmonary vascular disease rather than as a phenomenon secondary only to established vascular injury.

Among the platelet proteins potentially susceptible to DHP-mediated interference, the IP receptor is particularly relevant because prostacyclin signaling is a major endogenous inhibitory pathway that maintains platelet quiescence[21,22]. Targeted mass spectrometry demonstrated covalent DHP modification of the IP receptor, including residue H266 in rats, corresponding to the conserved H237 residue in humans. This structural modification was accompanied by reduced platelet cAMP levels, consistent with impaired IP receptor signaling. Rather than establishing irreversible receptor inactivation *per se*, these data support the concept that stable covalent modification of the IP receptor may contribute to sustained attenuation of its inhibitory signaling and thereby favor platelet activation following MCT exposure.

The functional relevance of this platelet-associated pathway was further supported by both *in vivo* and *in vitro* intervention experiments. In MCT-exposed rats, selexipag attenuated pulmonary arterial wall thickening, endothelial hyperplasia, medial smooth muscle hypertrophy, pulmonary PDGF-B accumulation, and vascular cell proliferation. In the platelet-RPASMC co-culture system, DHMCT increased P-selectin and PDGF concentrations, enhanced RPASMC proliferation, and increased phosphorylated PDGFR-β, PI3K, and AKT, whereas ACT-333679 attenuated these responses. These convergent findings strengthen the association between platelet activation, increased PDGF availability, and downstream proliferative signaling in pulmonary arterial smooth muscle cells. Importantly, however, selexipag and ACT-333679 are pharmacological agonists of IP receptor signaling rather than platelet-specific inhibitors, and PDGF measured in the co-culture system cannot be unequivocally assigned to platelets alone. Thus, the present data support a

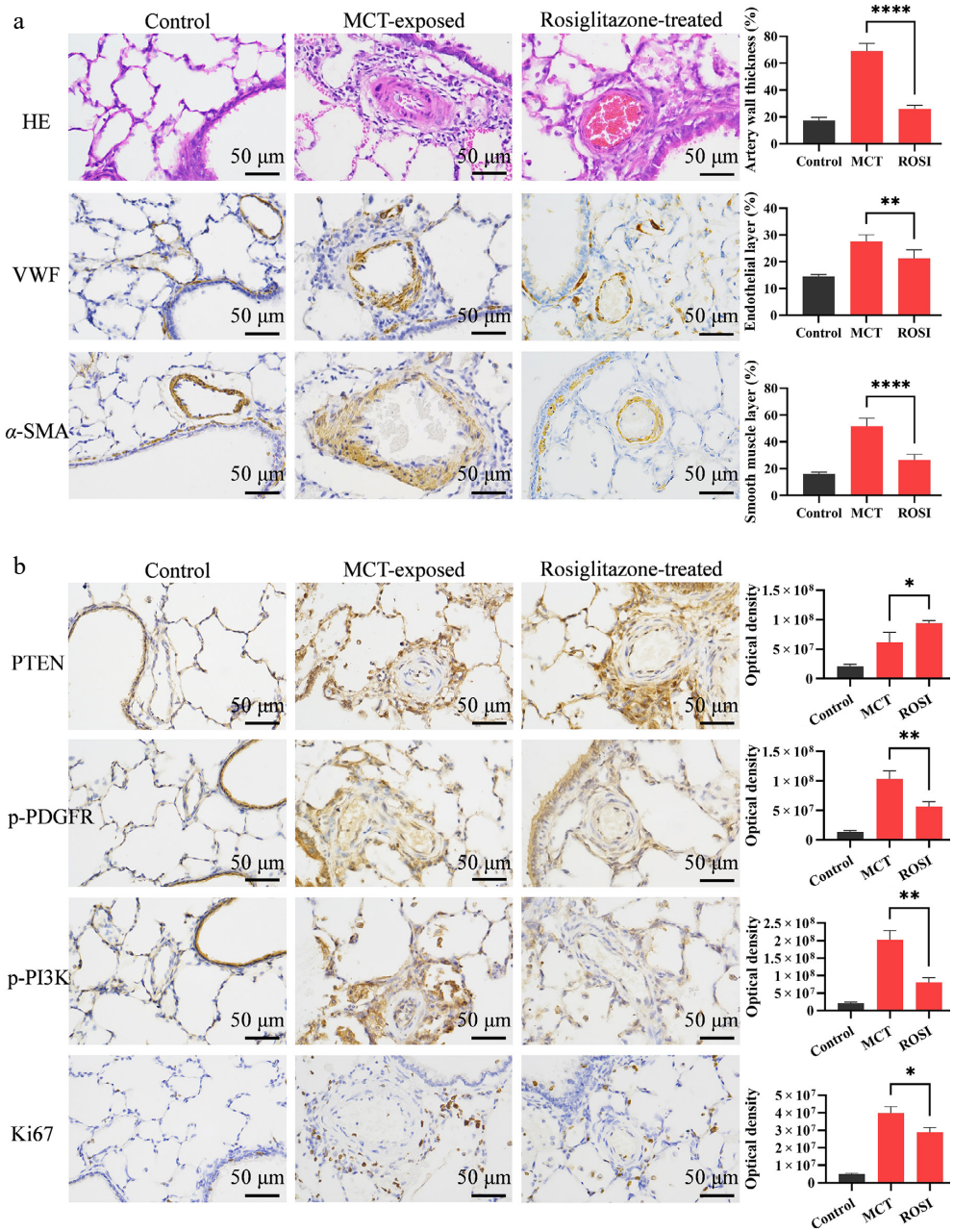


Fig. 7 Rosiglitazone alleviates pulmonary vascular remodeling by restoring PTEN expression and inhibiting the PDGFR/PI3K pathway. (a) Representative H&E and IHC (for vWF, α-SMA) images of lung tissues. ROSI treatment ameliorated MCT-induced pulmonary vascular remodeling, including reduced wall thickness, endothelial hyperplasia, and medial smooth muscle hypertrophy. (b) IHC staining and quantitative analysis of PTEN, p-PDGFR, p-PI3K, and Ki67 in lung tissues. ROSI intervention upregulated PTEN expression, suppressed p-PDGFR and p-PI3K levels, and consequently inhibited vascular cell proliferation as indicated by reduced Ki67. Data are presented as mean ± SD ($n = 3$). * $P < 0.05$, ** $P < 0.01$, *** $P < 0.001$, **** $P < 0.0001$ compared with the MCT-treated group (unpaired Student's *t*-test). Scale bar = 50 μm.

functional contribution of the platelet/IP receptor-PDGF axis but do not exclude additional effects of MCT on endothelial cells, smooth muscle cells, or other cellular sources of PDGF.

Beyond its systemic effects on platelets, DHP also appears to potentially perturb proliferative regulatory mechanisms within the lung. Untargeted proteomic profiling of lung tissues identified numerous candidate DHP-adducted proteins without prior target-specific enrichment. DisGeNET enrichment revealed several cancer-related disease categories, including anaplastic carcinoma, carcinomatosis, and undifferentiated carcinoma, suggesting that proteins involved in dysregulated cellular growth may represent biologically relevant DHP targets. This observation prompted us to focus on PTEN, a key negative regulator of growth-promoting signaling and an established suppressor of the PDGFR/PI3K pathway[23,24]. Targeted mass spectrometry subsequently confirmed covalent DHP modification of PTEN, including K125 and several additional conserved residues.

The functional significance of PTEN adduction is supported by its central role in restraining PDGFR/PI3K signaling. Variants involving several of the DHP-modified PTEN residues have been classified as pathogenic in UniProt[25,26], suggesting that modification of these structurally important sites may compromise PTEN function. In the present study, MCT exposure was accompanied by activation of PDGFR/PI3K signaling and increased vascular cell proliferation,

https://doi.org/10.48130/targetome-0026-0048

whereas pharmacological upregulation of PTEN with rosiglitazone suppressed this proliferative signaling and attenuated pulmonary vascular remodeling. These findings are consistent with the concept that DHP-mediated PTEN modification may weaken endogenous inhibitory control over the PDGFR/PI3K axis. Nevertheless, because PTEN phosphatase activity and the functional consequences of individual DHP-adducted residues were not directly measured, the precise impact of these modifications on PTEN enzymatic activity remains to be established. In addition, rosiglitazone is a PPARγ agonist with pleiotropic biological effects beyond PTEN regulation. Although rosiglitazone treatment was associated with increased PTEN expression and reduced PDGFR/PI3K pathway activation in our study, PTEN-independent mechanisms may also contribute to its protective effects. Future studies using PTEN-specific genetic manipulation or selective pathway modulation will be required to define the precise contribution of PTEN to the observed phenotype.

On the basis of these findings, we propose a cooperative 'dual-hit' model for PA-induced pulmonary vascular remodeling (Fig. 8). The first component occurs in the circulation, where DHP-mediated modification of platelet regulatory proteins, including the IP receptor, is associated with sustained platelet activation and increased availability of platelet-associated mitogenic mediators such as PDGF. The second component occurs within the pulmonary vascular environment, where DHP-mediated modification of PTEN may reduce inhibitory control over the PDGFR/PI3K signaling axis. Increased extracellular growth-factor signaling together with diminished intracellular inhibitory regulation could therefore converge to amplify pulmonary vascular cell proliferation and remodeling. This model does not exclude the well-established contribution of direct endothelial injury caused by MCT metabolites; rather, it expands the conventional endothelial-centric view by incorporating platelet dysregulation and loss of proliferative restraint as additional interacting mechanisms. Although DHP is a systemic reactive metabolite that may modify susceptible proteins in multiple tissues, our proposed model does not imply lung-exclusive targeting by DHP. Rather, we propose that pulmonary vascular remodeling results

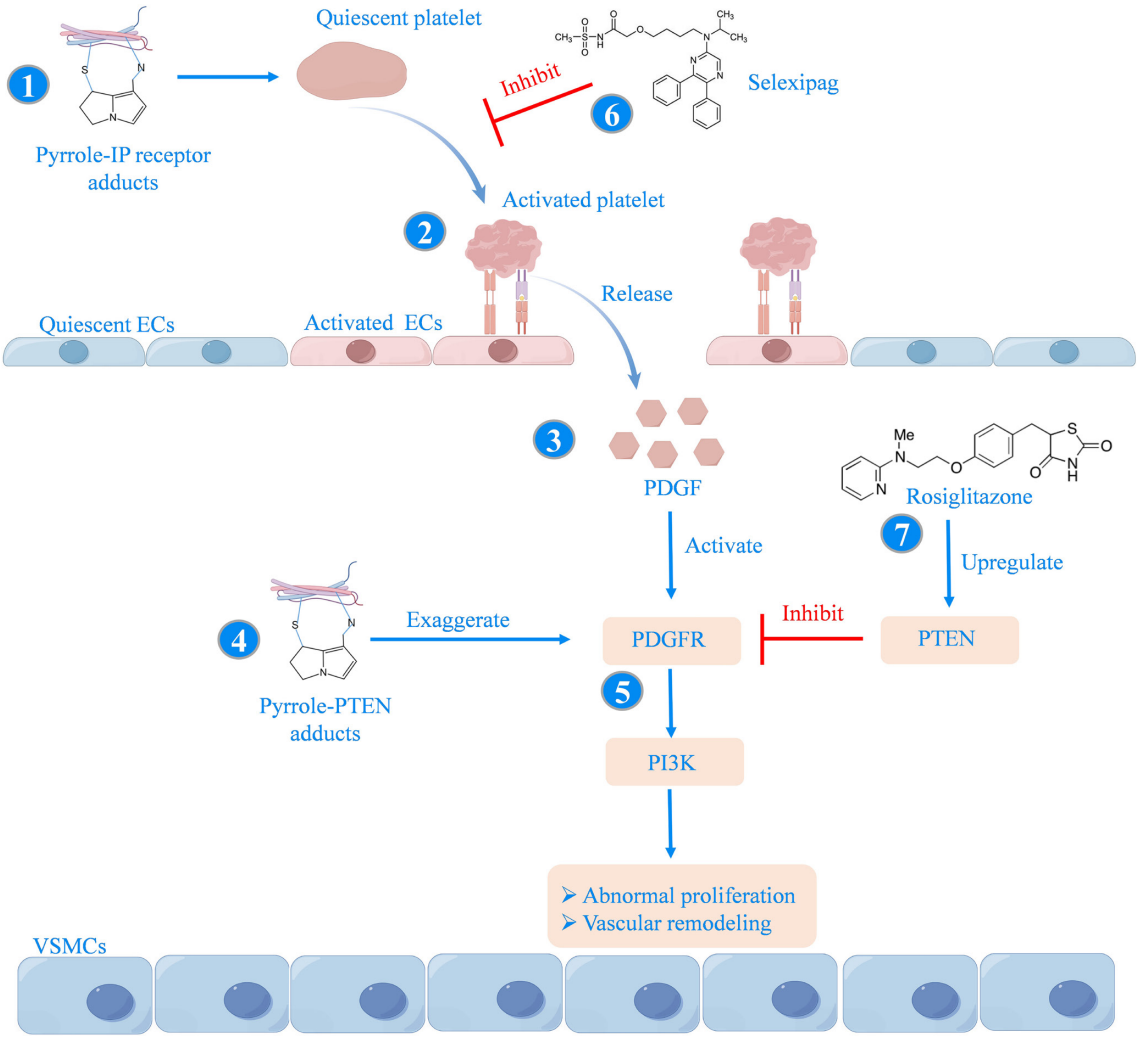


Fig. 8 Proposed mechanism of PA-induced PAH *via* covalent targeting of the IP receptor and PTEN and the corresponding therapeutic interventions. (1) Reactive PA metabolites (e.g., those derived from MCT) covalently modify the IP receptor through formation of pyrrole-IP receptor adducts, impairing IP receptor signaling and promoting platelet activation. (2) Activated platelets sequester in the pulmonary vasculature and release PDGF upon degranulation, leading to increased PDGF accumulation within the vascular wall. (3) Increased local PDGF levels promote activation of PDGFR signaling. (4) Simultaneously, reactive PA metabolites form pyrrole-PTEN adducts that impair PTEN function, thereby relieving its endogenous suppression of the PDGFR/PI3K axis. (5) The resulting activation of PDGFR/PI3K signaling promotes aberrant proliferation of pulmonary vascular cells and pathological vascular remodeling. (6) Pharmacological inhibition of platelet activation with selexipag decreases PDGF release, thereby attenuating PA-induced PAH. (7) Pharmacological upregulation of PTEN by rosiglitazone restores its inhibitory control over the PDGFR/PI3K pathway, thereby suppressing abnormal vascular cell proliferation and alleviating PA-induced PAH. Created with FigDraw.

from the convergence of systemic molecular alterations and pulmonary vascular susceptibility. MCT-induced PAH is a well-established model of pulmonary vascular toxicity, in which reactive DHP metabolites contribute to vascular injury and remodeling. In this context, systemic platelet dysregulation caused by IP receptor modification and local impairment of pulmonary proliferative control caused by PTEN modification may converge within the pulmonary vascular environment, where dysregulated PDGF/PDGFR signaling plays a critical role in vascular remodeling. Therefore, the pulmonary phenotype observed after MCT exposure likely reflects the interaction between systemic DHP exposure and pulmonary vascular vulnerability rather than selective modification of pulmonary tissues alone.

The pharmacological intervention experiments further highlight the therapeutic relevance of these pathways. Activation of IP receptor signaling with selexipag attenuated MCT-induced pulmonary vascular remodeling and reduced PDGF-B accumulation and vascular cell proliferation, whereas rosiglitazone treatment was associated with increased PTEN expression, reduced PDGFR/PI3K signaling activation, and attenuation of vascular remodeling. These findings suggest that targeting either the upstream platelet-associated component or the downstream loss of proliferative control may modify the progression of PA-induced pulmonary vascular disease. Similar to the selexipag intervention, rosiglitazone administration was initiated immediately after MCT exposure; therefore, these findings should be interpreted as an early-intervention strategy that attenuates disease development rather than a reversal treatment for established PAH.

From a broader public health perspective, natural product exposures, including PA-containing herbal medicines and contaminated foods, have recently been proposed as potentially underrecognized contributors to the global burden of PAH[11]. Although such ecological associations remain hypothesis-generating, they highlight the potential importance of environmentally and culturally patterned exposures in PAH epidemiology and reinforce the need to better define the molecular consequences of PA exposure in humans.

Several limitations should be considered. First, the present study was conducted primarily in a rodent model of MCT-induced PAH, and whether comparable DHP adduction of the IP receptor and PTEN occurs in patients exposed to PAs remains to be established. Second, although targeted mass spectrometry identified specific DHP-modified residues, functional studies using site-directed mutagenesis or direct enzymatic assays will be required to determine the contribution of individual adduct sites to IP receptor and PTEN dysfunction. Furthermore, although pyrrole-protein adduct levels decreased after 48 h, whether this reflects degradation, turnover, or clearance of reactive metabolites remains unclear. Future studies using proteasome inhibition or protein turnover assays are required to clarify the fate of DHP-modified proteins. Third, although selexipag intervention and platelet-RPASMC co-culture experiments provide convergent evidence supporting a platelet-associated PDGF signaling mechanism, selexipag and ACT-333679 are not platelet-specific, and the cellular origin of pulmonary PDGF-B was not directly lineage-traced. Finally, PTEN regulates multiple signaling pathways beyond PDGFR/PI3K, including AKT- and MAPK-related networks, and the contribution of these additional pathways to DHP-induced vascular remodeling warrants further investigation.

In conclusion, our findings support an integrated model in which DHP-mediated covalent modification of platelet and pulmonary regulatory proteins contributes to MCT-induced PAH. Covalent modification of the platelet IP receptor is associated with sustained platelet activation, whereas modification of pulmonary PTEN may weaken inhibitory control over proliferative PDGFR/PI3K signaling. These findings reveal a previously unrecognized mechanism whereby reactive environmental metabolites induce disease-associated signaling abnormalities through site-specific covalent protein modification. Together with the effects of selexipag, ACT-333679, and rosiglitazone observed *in vivo* and *in vitro*, these data identify the platelet/IP receptor-PDGF axis and PTEN-regulated proliferative signaling as interacting molecular processes that may contribute to PA-induced pulmonary vascular remodeling and represent potential targets for therapeutic intervention.

Ethical statements

This research was carried out following the formal approval of the Animal Ethics Committee of The Chinese University of Hong Kong, Shenzhen (Approval No. CUHKSZ-AD-20230047, approval date: 2023.03.28). All animal-related procedures complied with the recognized guidelines for the care and welfare of laboratory animals.

Author contributions

The authors confirm their contributions to the paper as follows: study conception and design, manuscript revision and editing: He Y; data collection: Zhang C, Guo X, Huang T; analysis and interpretation of results: Zhang C, Guo X, Huang T, Fan Y; draft manuscript preparation: Zhang C. All authors reviewed the results and approved the final version of the manuscript.

Data availability

All data generated or analyzed during this study are included in this published article and its supplementary information files.

Acknowledgments

This work was supported by the National Natural Science Foundation of China (No. 82474179), the Guangdong Basic and Applied Basic Research Foundation (No. 2024A1515011705, 2023A1515110677), the Foundation of Shenzhen Science and Technology Innovation Commission (No. JCYJ20240813113552066), and the Hospital University United Fund of The Second Affiliated Hospital, School of Medicine, The Chinese University of Hong Kong, Shenzhen (HUUF-MS-202301).

Conflict of interest

The authors declare that they have no conflict of interest.

Supplementary information accompanies this paper online at: https://doi.org/10.48130/targetome-0026-0048.

Dates

Received 9 May 2026; Revised 27 August 2026; Accepted 1 September 2026; Published online 23 September 2026

References

[1] Ruopp NF, Cockrill BA. 2022. Diagnosis and treatment of pulmonary arterial hypertension: a review. *JAMA* 327:1379–1391

[2] Tuder RM. 2009. Pathology of pulmonary arterial hypertension. *Seminars in Respiratory and Critical Care Medicine* 30:376–385

[3] Simonneau G, Gatzoulis MA, Adatia I, Celermajer D, Denton C, et al. 2013. Updated clinical classification of pulmonary hypertension. *Journal of the American College of Cardiology* 62:D34–D41

[4] Humbert M, Sitbon O, Guignabert C, Savale L, Boucly A, et al. 2023. Treatment of pulmonary arterial hypertension: recent progress and a look to the future. *The Lancet Respiratory Medicine* 11:804–819
[5] Mandras SA, Mehta HS, Vaidya A. 2020. Pulmonary hypertension: a brief guide for clinicians. *Mayo Clinic Proceedings* 95:1978–1988
[6] Thenappan T, Ormiston ML, Ryan JJ, Archer SL. 2018. Pulmonary arterial hypertension: pathogenesis and clinical management. *BMJ* 360:j5492
[7] Beshay S, Guha A, Sahay S. 2021. Evaluation, diagnosis, and classification of pulmonary hypertension. *Methodist DeBakey Cardiovascular Journal* 17:86–91
[8] Zhang C, Song Z, Zhao Y, Guo X, Huang T, et al. 2025. The underexplored pulmonary toxicity of pyrrolizidine alkaloids: emerging hazard from food contamination. *Chemico-Biological Interactions* 420:111709
[9] Schrenk D, Gao L, Lin G, Mahony C, Mulder PPJ, et al. 2020. Pyrrolizidine alkaloids in food and phytomedicine: occurrence, exposure, toxicity, mechanisms, and risk assessment - a review. *Food and Chemical Toxicology* 136:111107
[10] Brugnerotto P, Silva B, Gonzaga LV, Costa ACO. 2025. Comprehensive review of pyrrolizidine alkaloids in bee products: occurrence, extraction, and analytical methods. *Food Chemistry* 483:144211
[11] Zhang C, Huang T, Guo X, Cui X, He Y. 2026. Hemolysis-associated disorder and natural product exposures: underrecognized drivers of an escalating global pulmonary arterial hypertension burden—an ecological study of 204 countries and territories. *Future Integrative Medicine* 1–17
[12] Hill NS, Gillespie MN, McMurtry IF. 2017. Fifty years of monocrotaline-induced pulmonary hypertension: what has it meant to the field? *Chest* 152:1106–1108
[13] Zhang C, Huang T, Guo X, Fan Y, Song Z, et al. 2026. Hemoglobin adduction and impaired oxygen transport define the etiology of pyrrolizidine alkaloid-induced pulmonary arterial hypertension. *Phytomedicine* 152:157847
[14] Solinc J, Ribot J, Soubrier F, Pavoine C, Dierick F, et al. 2022. The platelet-derived growth factor pathway in pulmonary arterial hypertension: still an interesting target? *Life* 12:658
[15] Amelirad A, Shamsasenjan K, Akbarzadehlaleh P, Pashoutan Sarvar D. 2019. Signaling pathways of receptors involved in platelet activation and shedding of these receptors in stored platelets. *Advanced Pharmaceutical Bulletin* 9:38–47
[16] Estevez B, Du X. 2017. New concepts and mechanisms of platelet activation signaling. *Physiology* 32:162–177
[17] Pullamsetti SS, Savai R, Seeger W, Goncharova EA. 2017. Translational advances in the field of pulmonary hypertension. From cancer biology to new pulmonary arterial hypertension therapeutics. Targeting cell growth and proliferation signaling hubs. *American Journal of Respiratory and Critical Care Medicine* 195:425–437
[18] Cai B, Yang L, Do Jung Y, Zhang Y, Liu X, et al. 2022. PTEN: an emerging potential target for therapeutic intervention in respiratory diseases. *Oxidative Medicine and Cellular Longevity* 2022:4512503
[19] Song Z, Lian W, He Y, Zhang C, Lin G. 2023. Targeting erythrocyte-mediated hypoxia to alleviate lung injury induced by pyrrolizidine alkaloids. *Archives of Toxicology* 97:819–829
[20] Ma J, Ruan J, Chen X, Li D, Yao S, et al. 2019. Pyrrole-hemoglobin adducts, a more feasible potential biomarker of pyrrolizidine alkaloid exposure. *Chemical Research in Toxicology* 32:1027–1039
[21] Offermanns S. 2006. Activation of platelet function through G protein–coupled receptors. *Circulation Research* 99:1293–1304
[22] Bye AP, Unsworth AJ, Gibbins JM. 2016. Platelet signaling: a complex interplay between inhibitory and activatory networks. *Journal of Thrombosis and Haemostasis* 14:918–930
[23] Green DE, Sutliff RL, Hart CM. 2011. Is peroxisome proliferator-activated receptor gamma (PPARγ) a therapeutic target for the treatment of pulmonary hypertension? *Pulmonary Circulation* 1:33–47
[24] Mahimainathan L, Choudhury GG. 2004. Inactivation of platelet-derived growth factor receptor by the tumor suppressor PTEN provides a novel mechanism of action of the phosphatase. *Journal of Biological Chemistry* 279:15258–15268
[25] Apweiler R, Bairoch A, Wu CH, Barker WC, Boeckmann B, et al. 2004. UniProt: the universal protein knowledgebase. *Nucleic Acids Research* 32:D115–D119
[26] McGarvey PB, Nightingale A, Luo J, Huang H, Martin MJ, et al. 2019. UniProt genomic mapping for deciphering functional effects of missense variants. *Human Mutation* 40:694–705
[27] Teresi RE, Shaiu CW, Chen CS, Chatterjee VK, Waite KA, et al. 2006. Increased PTEN expression due to transcriptional activation of PPARγ by Lovastatin and Rosiglitazone. *International Journal of Cancer* 118:2390–2398
[28] Kato S, Ohnuma N, Ohno K, Takasaki K, Okamoto S, et al. 1997. Changes in sequestered leukocytes and platelets in the pulmonary microvasculature of rats with monocrotaline-induced pulmonary hypertension. *International Journal of Microcirculation: Clinical and Experimental* 17:290–297
[29] Hu XS, Du CQ, Zeng CL, Yao L, Zhang FR, et al. 2010. Systemic evaluation of platelet and leukocyte activation and interaction in a rat model of pulmonary arterial hypertension. *Cardiology* 117:44–53
[30] Ono S, Voelkel NF. 1991. PAF antagonists inhibit monocrotaline-induced lung injury and pulmonary hypertension. *Journal of Applied Physiology* 71:2483–2492
[31] Zhu Y, Shu D, Gong X, Lu M, Feng Q, et al. 2022. Platelet-derived TGF (transforming growth factor)-β1 enhances the aerobic glycolysis of pulmonary arterial smooth muscle cells by PKM2 (pyruvate kinase muscle isoform 2) upregulation. *Hypertension* 79:932–945

Copyright: © 2026 by the author(s). Published by Maximum Academic Press on behalf of China Pharmaceutical University. This article is an open access article distributed under Creative Commons Attribution License (CC BY 4.0), visit https://creativecommons.org/licenses/by/4.0/.